XX. APPLIED PLASMA RESEARCH*

A. Active Plasma Systems

Academic and Research Staff

Prof. L. D. Smullin
Prof. R. J. Briggs
Prof. R. R. Parker
Prof. K. I. Thomassen

Graduate Students

Y. Ayasli
D. S. Guttman
R. K. Linford
J. A. Mangano
J. A. Rome
M. D. Simonutti

RESEARCH OBJECTIVES

The research of the Active Plasma Systems Group is primarily concerned with the behavior of highly ionized plasmas and charged-particle beams. Several experimental investigations related to plasma heating in a beam-plasma discharge are under way, and the studies of feedback stabilization of plasma instabilities begun during the past year are receiving an increasing amount of attention. A discussion of some of these individual topics follows.

1. Stability of Sheared Electron Flow

During the past year a number of particular velocity profiles in a magnetically confined beam were analyzed for stability. We have developed a computer program that efficiently maps the stability boundaries and growth rates, and during the coming year we plan to continue the stability analysis of magnetically confined beams, and also to consider the generalization to finite focusing magnetic fields and to relativistic beams.

R. J. Briggs

2. Feedback Stabilization in Plasmas

During the past year we stabilized the drift-type instability of a reflex discharge by feedback stabilization. Our objectives now are to investigate different ways to couple to these modes, to correlate theory and experiment, and more generally to explore the usefulness of this stabilization scheme against other instabilities.

R. R. Parker, K. I. Thomassen

3. Electric Arc Thruster Study†

A vacuum arc thruster using solid teflon fuel is being investigated. Our objective is to understand the physics of this arc discharge and to model the device to be able to predict and improve performance.

K. I. Thomassen

---

*This work was supported by the National Science Foundation (Grant GK-10472).

†This work is supported by Lincoln Laboratory, M. I. T. (P. O. No. A-3393).

4. Stochastic Heating of Plasma

The purpose of this project is to explore ways to heat a plasma with externally applied random RF fields. Of particular interest is the efficiency and uniformity of stochastic heating vs that obtained with traditional coherent heating methods. At present, we are constructing a Lusitano coil to couple high-power broadband noise in the ultrahigh-frequency band to a plasma in a nonuniform magnetic field. Another experiment is concerned with stochastic excitation of the low-frequency ion-cyclotron wave using a specially designed broadband RF coupling structure. In this experiment, measurements of the ion distribution function are being made and will be compared with the results of coherent excitation.

K. I. Thomassen, R. R. Parker

5. Radiation and Turbulence in Beam-Plasma Discharge

During the past year, we have continued investigation of the radiated RF spectrum generated by the beam-plasma interaction. Our objective has been primarily to determine the role that mode-coupling phenomena might play in shaping the low-frequency spectrum. While there is ample theoretical reason to believe that this should be present, the experimental evidence is still inconclusive. To help resolve the situation, we have designed a set of microwave arrays that will be used during the coming year in microwave scattering experiments. In this way, spatial, as well as temporal, resolution of the spectrum of density fluctuations will be obtained.

L. D. Smullin, R. R. Parker

1. ION CYCLOTRON RESONANCE HEATING

An experiment to study certain aspects of ion cyclotron resonance heating in a beam-plasma discharge has been set up and has yielded some preliminary results. A description of the experiment is given here.

The purpose of the experiment is to examine the differences in the power absorption process when excitation of RF power is applied at a single frequency, is applied at two distinct frequencies, or ultimately over a band of frequencies by means of modulation of the signal by a noise source. It is believed that excitation over a band of frequencies would be of advantage because the ion cyclotron resonant absorption region is spread out in space rather than confined to a thin sheet, and also because the thermalization of ions is improved. A study of the wave absorption process at resonance has been made by Kuckes.[1]

Extensive theoretical and large-scale experimental studies on ion cyclotron heating at a single frequency have been in progress at the Plasma Physics Laboratory of Princeton University. This work has shown that this method of heating is promising in fusion-machine[2] applications.

The magnetic field of the system is in a mirror configuration with a mirror ratio ≈ 3 and a magnetic field ≈ 6 kG at the mirror peak. An RF induction coil is wound around a 3.5 in. diameter glass tube that surrounds the plasma at the collector end of the beam plasma system and is located directly under the mirror peak. The coil and vacuum

capacitors form a tank circuit tuned to 6 MHz and having a Q of ~200. At present, a 1.7 kW RF amplifier is used to excite the circuit at a single frequency. This excitation launches ion cyclotron waves that propagate in the hydrogen plasma toward the center of the system in a decreasing magnetic field.[3] When the wave reaches the resonance point where the excitation frequency passes from below the local cyclotron frequency to a point equal to the local cyclotron frequency the wave power is nearly completely absorbed and converted into ion perpendicular kinetic energy.[3] This process is characteristic of wave propagation through a medium in which the refractive index has an infinity or resonance.

Measurements of the wave amplitude indicate that approximately 10% of the power from the RF amplifier is converted into wave power, with most of the remaining power being lost to dissipation in the tank circuit.

To obtain an indication of the ion energy of the plasma, a retarding potential analyzer is placed at the collector end of the system on the axis of the system and within the hollow cylindrical electron beam. The output of the analyzer is a current that can be monitored on an oscilloscope. The current is given by the expression

$$I_c = e \int_{e\phi}^{\infty} A(W_{||})\, f_{||}(W_{||}, z = w)\, v_{||}(W_{||})\, dW_{||},$$

where $f_{||}(W_{||}, z=w)$ is the parallel energy distribution function normalized by the spatial density n_o; $A(W_{||})$ is the effective entrance area of the analyzer which actually is a function of the orbit of the ions but may be considered constant; the axis of the system is in the z direction and the analyzer is placed at $z = w$; and $v_{||}$ is the parallel component of ion velocity given simply by

$$v_{||} = \left(\frac{2W_{||}}{m}\right)^{1/2}.$$

The analyzer measures ion current contributed by ions with velocity directed toward the analyzer. Because the analyzer is placed at the mirror peak, however, and because there is an electrostatic potential in the plasma that drives the ions out of the system, all ions at $z = w$ have velocities directed toward the analyzer.[4]

The absorbed wave power is converted directly to perpendicular ion energy, while the analyzer measures only parallel energy. There is always some conversion to parallel energy, however, through collisions in the plasma. Therefore the analyzer should be useful in giving some indication of the effects of our RF heating. It must be understood that precise interpretation of the data from the analyzer is extremely difficult because of the indirect way in which it gives information about perpendicular ion energy and because of the existence of the electrostatic potential in the machine

which distorts the ion energy distribution.

A typical plot of analyzer current against retarding potential from our experiment as it now exists is given in Fig. XX-1. Although the effect of the radio frequency is small because of the limited RF power available, it is evident.

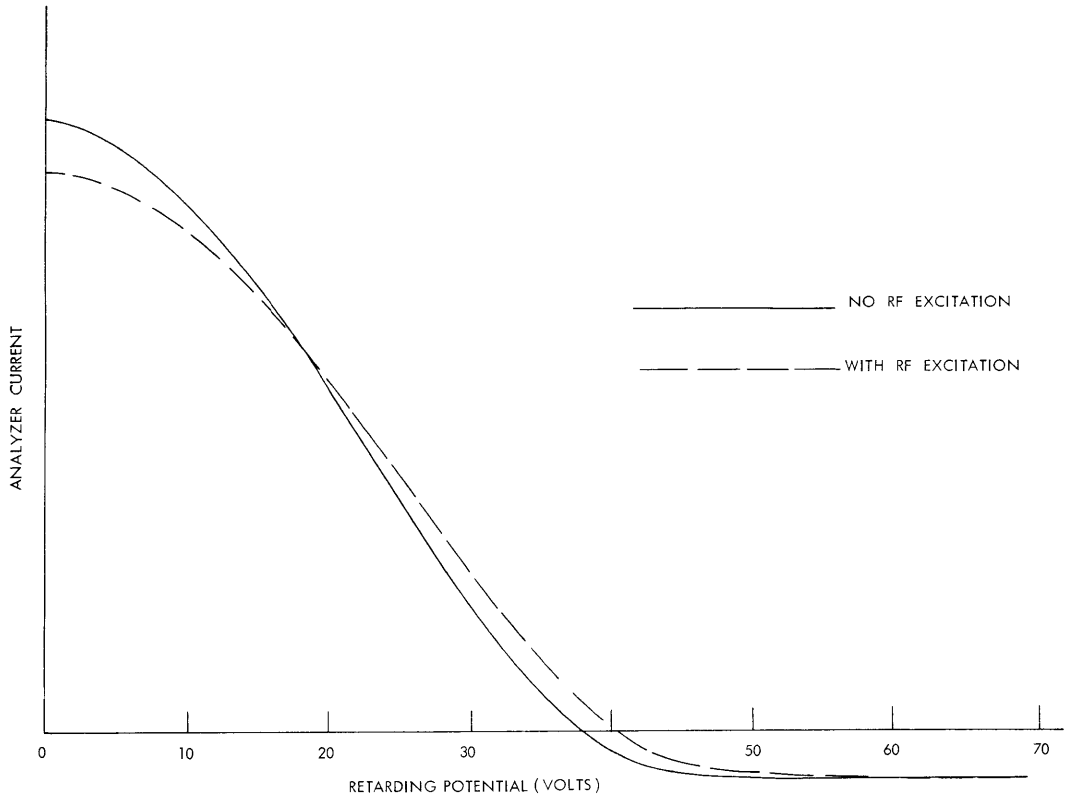

Fig. XX-1. Retarding potential analyzer current vs voltage.

The tail of the curves gives most information about actual ion energy because the current at lower retarding voltage is mainly determined by the static potential in the machine, a potential that varies from approximately +25 V at the center of the machine to approximately +10 V at the mirror peak.

We see that the tail of the curve obtained with RF heating applied is above the one without RF, thereby indicating the presence of more higher energy ions.

The acceleration fields of the wave increase from zero with increasing radius in the plasma. Thus we believe that the ions measured with increased energy from RF heating reach the axis of the system where the analyzer is mounted by a diffusion process. Placing the analyzer at the outer edge of the electron beam rather than on-axis concentric with the beam should yield clearer results. This change

in the system is now in progress.

Examination of the signal from a diamagnetic coil around the plasma column has not been successful as an indication of ion energy. The presence of high-energy electrons trapped between the mirrors dominate the diamagnetic signal greatly. The changes in the ion perpendicular energy, small because of the limited RF power, have been impossible to detect over the noise that is present on the signal.

After single-frequency operation of the system has been well studied, heating at two distinct frequencies and then over a frequency band will be put into operation and investigated.

M. D. Simonutti, R. R. Parker

References

1. A. F. Kuckes, "Resonant Absorption of Electromagnetic Waves in a Non-uniformly Magnetized Plasma," Plasma Phys. 10, 367-380 (1968).
2. M. A. Rothman, R. M. Sinclair, I. G. Brown, and J. C. Hosea, "Ion Cyclotron Heating in a Model C Stellarator," Report MATT-606, Plasma Physics Laboratory, Princeton University, January 1969.
3. T. H. Stix, Theory of Plasma Waves (McGraw-Hill Book Company, New York, 1962), Chap. 5.
4. R. K. Linford, "Ion Energy Analysis in a Beam Plasma Discharge," S.M. Thesis, Department of Electrical Engineering, M.I.T., March 1969.

2. MEASUREMENT OF THE WAVE-NUMBER SPECTRUM OF A BEAM-PLASMA DISCHARGE

Since their inception, beam-plasma discharges have been subjected to numerous investigations of the spectra of the fluctuating fields resulting from the beam-plasma interaction. Such studies have been mainly concerned with frequency analysis, and have often resulted in ambiguous interpretation, because of the large number of modes that are possible in this complex phenomenon. This ambiguity is due to the fact that frequency analysis is only one side of the coin, the other being wave-number analysis. Thus, at a given frequency an infinite number of modes of propagation may exist, but each is distinguished by different values of wave number. Hence it is clear that a much more complete experimental picture of the phenomena can be put together if we have knowledge of both frequency and wave-number spectra.

A convenient tool which can be used for wave-number analysis of a fluctuating medium is microwave scattering. This is essentially Bragg scattering, in which the Bragg planes are caused by the regular compressions and refractions of the plasma density produced by a coherent wave propagating through the plasma. If the plasma can be properly thought of as turbulent, the scattering is due to Fourier components

of the correlation function. In any case, a systematic measurement of the microwave power scattered by the plasma can be used to obtain quantitative information about the wave-number decomposition of the fluctuations taking place in the plasma.

We have begun work on a program that has as its objective such a systematic measurement of microwave scattering by a beam-generated plasma. It was quite clear at the outset that the problem of measuring wave-number spectra is considerably more difficult than that of measuring frequency spectra, since the resolution obtainable in any practical configuration is severely limited by factors, such as size of the scattering volume, dimensions of the incident and scattered microwave beams, and other limitations imposed by the geometry of the experiment. It is these aspects of the problem that we shall discuss in this report.

We consider a fluctuating plasma with a dielectric constant $\epsilon(\vec{r}, t) = \epsilon_o + \Delta\epsilon(\vec{r}, t)$, and make the single-scatter or Born approximation. The statistical properties of the scattered field will be related to the statistics of the turbulent medium causing the scattering. We make the assumption that the statistics themselves are not changing during the measurements; that is, they are "locally stationary." In this way, the statistical problem could be solved as though the process is truly stationary and the slowly changing statistics could be accounted for afterward.[1] Also, we assume that $\Delta\epsilon$ varies slowly in time compared with the incident microwave frequency ω_o.

The average scattering cross section of a turbulent plasma of volume V illuminated by a plane electromagnetic wave is given by[2]

$$\sigma = \sin^2 \Omega \, r_e^2 \int_V \int_V \langle \Delta\epsilon(\vec{r}_1, t_1)\Delta\epsilon(\vec{r}_2, t_2)\rangle \cdot \exp[-(\vec{k}_i - \vec{k}_s)\cdot(\vec{r}_1 - \vec{r}_2)] \, dV_1 dV_2, \qquad (1)$$

where

σ = scattering cross section; power scattered per unit incident Poynting flux, unit solid angle, in the scattered direction.

$\vec{k}_i, \vec{k}_s$ = incident, scattered wave vector.

r_e = classical electron radius.

V_1, V_2 = volume; subscripts represent two independent integrations.

Ω = angle between $\vec{k}_s$ and incident polarization.

$\langle \Delta\epsilon(\vec{r}_1, t_1)\Delta\epsilon(\vec{r}_2, t_2)\rangle$ = correlation function of the fluctuations in time and space.

Under the assumption of a stationary random process, the correlation function can be written

$$\langle \Delta\epsilon(\vec{r}_1, t_1)\Delta\epsilon(\vec{r}_2, t_2)\rangle = \langle \Delta\epsilon\rangle^2 C(\vec{r},\tau) = \lim_{\substack{T\to\infty \\ V\to\infty}} \frac{1}{VT}\int d\vec{x}\int dt\ [\langle \Delta\epsilon(\vec{x},t)\Delta\epsilon(\vec{x}+\vec{r},t+\tau)\rangle],$$

where $C(\vec{r},\tau)$ is the normalized correlation function. In terms of its Fourier transform, it can be written

$$C(\vec{r},\tau) = \int \frac{d\omega}{2\pi} e^{j\omega\tau}\int \frac{d\vec{k}}{(2\pi)^3} e^{j\vec{k}\cdot\vec{r}}\, S(\vec{k},\omega)$$

which, together with Eq. 1 gives

$$\sigma(\vec{r},t) = \sin^2\Omega\ r_e^2\int_{-\infty}^{\infty} S(\vec{k},\omega-\omega_o)\, d\vec{k}\int_V \frac{e^{j(\vec{k}-\vec{k}_p)\cdot\vec{r}}}{(2\pi)^3}\, dV_r. \tag{2}$$

$S(\vec{k},\omega-\omega_o)$ is defined as the spectral density of fluctuations, and $\vec{k}_p = \vec{k}_s - \vec{k}_i$. The region of integration is limited to the region from which most of the power is scattered into the receiver.[1] Therefore V is limited to the common region of illumination of the two antennas, and to the region where $\langle \Delta\epsilon(r)^2\rangle$ is nonzero, that is, to the volume of turbulence.

The last integral on the right-hand side of Eq. 2 tends to $\delta(\vec{k}-\vec{k}_p)$ as $V \to \infty$. The scattering cross section is thus proportional to the power spectral density, weighted by this integral. In this sense, it acts as a filter with a bandwidth of the order of $8\pi^3/V$ and centered at $\vec{k} = \vec{k}_p$. Thus the scattered power in the $\vec{k}_s$ direction is determined by the fluctuation wave vectors that are spaced[3] around $(\vec{k}_s-\vec{k}_i)$. On the other hand, frequency resolution can be obtained by sending the received signal through a frequency analyzer. Thus it should theoretically be possible to determine the fluctuation frequencies as a function of $\vec{k}_p$.

From the argument above, it is clear that the actual response of this filter is determined by the geometry of the scattering volume. For the cylindrical geometry that will be used for the actual measurements, it is easy to see that scattering can occur only from axial fluctuations if the angle between $\vec{k}_i$ and the z axis is kept equal to the angle between $\vec{k}_s$ and the z axis. In this way, normalization factors attributable to the radial wave numbers can be eliminated, so that $\vec{k}_p = -\hat{i}_z 2k\cos\theta = -\hat{i}_z 2k_{||}$, as shown in Fig. XX-2.

Some of these results have been verified on a dielectric plasma model at 70 GHz. In order to do the actual measurements on a plasma, we have designed two identical X-band arrays each of which has 30 longitudinal slots on the broad fact of a waveguide. The wave number parallel to the axis of the waveguide is given by

$$k_{||} = \beta - (2n+1)\frac{\pi}{L},$$

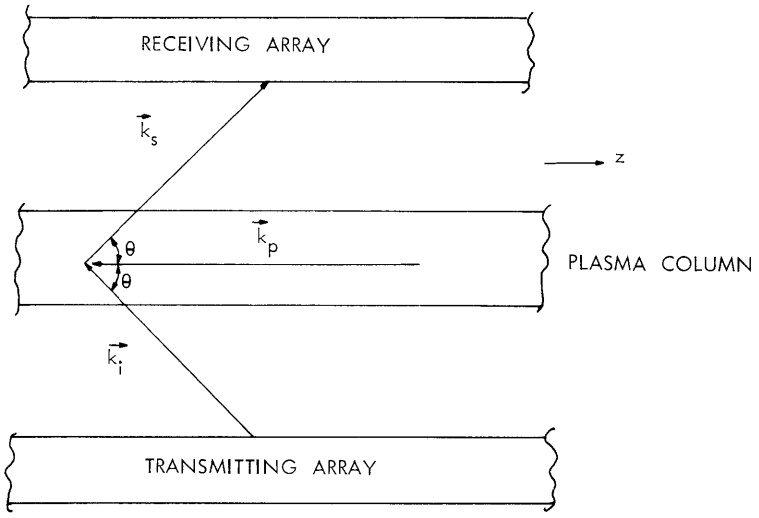

Fig. XX-2. Microwave scattering experiment.

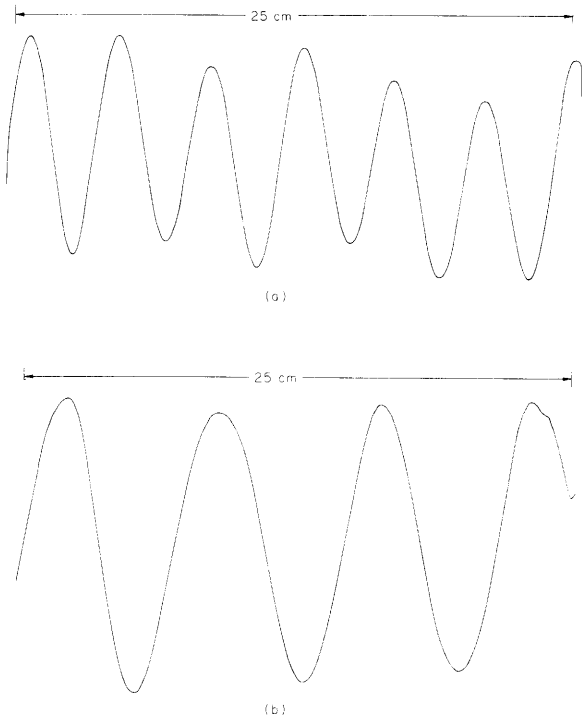

Fig. XX-3. Measurements of $k_{||}$ produced by an X-band array at two frequencies: (a) f_o = 8.9 GHz, $k_{||}$ = 0.8 cm^{-1}; (b) f_o = 10.0 GHz, $k_{||}$ = 0.45 cm^{-1}. The results of scattering experiments should be proportional to the squared magnitude of the Fourier transform of these plots. Hence the bandwidth of the "wave-number analyzer" is determined by the degree to which these plots are sinusoidal. End effects will also play an important role, but these are not shown in these plots.

where β is the wave number inside the waveguide, L is the center-to-center slot separation, and n is any integer. By a suitable choice of L and β, only the mode corresponding to n = 0 is allowed to propagate. Thus for this particular array

$$k_{||} = \beta - \frac{\pi}{L} \quad \text{and} \quad k_p = 2\left(\beta - \frac{\pi}{L}\right).$$

By varying the frequency of the X-band generator, it is possible to cover the wave numbers from approximately 0.9 cm^{-1} to very small values, which corresponds to wavelengths of ~3.5 cm and longer.

It has been shown that a scattered signal will be received by the receiver if there is a fluctuation wave number around $2k_{||}$ in the turbulent-plasma medium. Thus in order to improve the resolution, it is important to produce a $k_{||}$ that is as close to a single wave number as possible. The $k_{||}$ of the arrays constructed has been measured as a function of frequency by moving a conducting bead along the axis of the array. Using reciprocity, it can be shown that the backscattered signal amplitude is proportional to $e^{j2k_{||}z}$. As the bead is moved along the z axis with a constant velocity, the amplitude modulation of the backscattered signal is recorded to determine $2k_{||}$. Two of these array patterns are shown in Fig. XX-3, so that the change in $k_{||}$ can be observed for two different frequencies. These arrays will be used for measurements on a beam-plasma discharge.

Y. A. Ayasli, R. R. Parker

References

1. M. Balser, IRE Trans., Vol. AP-1, pp. 383-390, 1957.
2. T. E. Luzzi, IEEE Trans., Vol. AP-17, pp. 342-347, 1969.
3. V. I. Tatavski, Wave Propagation in a Turbulent Medium (Dover Publications, Inc., New York, 1967).

3. FEEDBACK STABILIZATION IN PLASMAS

The low-frequency instabilities of a reflex discharge[1] have been stabilized by feedback control,[2] using a Langmuir probe pickup, a wideband (100 kHz) amplifier and phase shifter, and plates spaced azimuthally around the glass discharge wall (inside). We shall present a simple slab model calculation predicting the stabilizing effect of feedback.

To describe the instability, we assume that the ions are cold, and that the pressure gradient on the electron is balanced by diamagnetism, not by the radial electric field that we take to be zero. Figure XX-4 shows the coordinate system, with

$|\nabla n| < 0$. From $nq\bar{v} \times \bar{B} = kT_e \bar{\nabla} n$ we find that the electron diamagnetic velocity $\bar{v} = (kT_e/qB) \frac{\bar{B} \times \bar{\nabla} n}{nB}$ is in the y direction.

From the ion continuity and momentum equations, we have

$$j\omega n_i + n_o \nabla \cdot v_i + v_i \cdot \nabla n_o = 0$$

$$\nabla \cdot v_i \cong -j \frac{e\phi}{m_i \omega} k_z^2 \qquad \omega \ll \omega_{ii}$$

$$v_{ix} \approx \frac{j k_y \phi}{B}$$

which give

$$\frac{n_i}{n_o} = \frac{e\phi}{kT_e} \left[\frac{k_z^2 C_s^2}{\omega^2} + \frac{\omega^*}{\omega} \right], \tag{1}$$

where $C_s^2 = kT_e/m_i$, $\omega^* = k_y |v_{De}|$. If (1) is equated with $n_e/n_o = e\phi/kT_e$, we find stable ion acoustic waves coupled to drift waves.

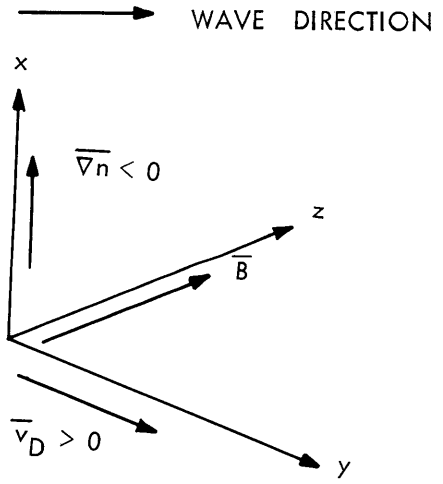

Fig. XX-4. Slab model showing magnetic field, density gradient, and diamagnetic velocity.

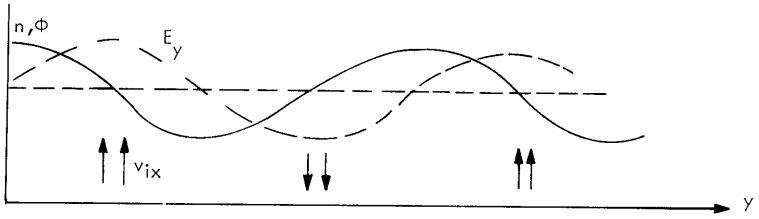

Fig. XX-5. Density, potential, field, and x-directed ion velocity variation.

A physical picture emerges from these equations, as shown in Fig. XX-5. If $\phi = A \cos k_y y$, $E_y = B \sin k_y y$ and $v_{ix} = C \sin k_y y$. The density is in phase with ϕ. We neglect ion compressibility (no acoustic wave). The density perturbation is being fed where $n = 0$ and E_y is maximum. Soon after this the density will increase there, so the wave moves to the right as predicted by $\omega = \omega^*$ $(k_z = 0)$. The wave is stable because $\langle nv_{ix} \rangle = 0$ over a full period. To make the wave unstable, particles must be transported along the x axis, so n and E_y must have an in-phase component. This requires n_e/n_o to be of the form $(1+j\alpha)e\phi/kT_e$.

If collisions are included in the electron motion, we find

$$\frac{n_e}{n_o} = \frac{e\phi}{kT_e} \frac{\left(k_z^2+k_y^2/M^2\right)D + j\omega^*}{\left(k_z^2+k_y^2/M^2\right)D + j\omega}, \tag{2}$$

where $D = kT_e/m\nu_e$, $M = \omega_{ce}/\nu_e$. Obviously, the required form for instability is obtained when $\omega < \omega^*$. For $\omega > \omega^*$ the waves damp because $\langle nE_y \rangle$ is directed along $-x$, feeding particles to the discharge from the outside. (The radial direction is x, the azimuthal is y.)

Feedback can be incorporated in the way demonstrated by Simonen, Chu, and Hendel.[3] The electron continuity equation will contain a source of electrons proportional to n_e. The plates at the wall subtract electrons at the rate governed by the feedback signal from the probe. So,

$$j\omega n_e + \nabla \cdot (nv)_e = \omega_f n_e,$$

where ω_f is the amplitude and phase of the proportionality constant determining the amount of injected or removed electron perturbation. Note that (2) has $j\omega$ in the denominator, so we simply replace it by $j\omega - \omega_f$, which requires $j\omega - \omega_f > j\omega^*$ for stability. If the phase of ω_f is imaginary (270°), then we require $(\omega_f)_{imag} > \omega^*$, which we can do by adjusting the gain and phase of the amplifier.

K. I. Thomassen

References

1. K. I. Thomassen, J. Appl. Phys. 39, 5017 (1968).
2. R. R. Parker and K. I. Thomassen, Phys. Rev. Letters 22, 1171 (1969).
3. T. C. Simonen, T. K. Chu, and H. W. Hendel, Phys. Rev. Letters 23, 568 (1969).

4. ELECTRIC ARC THRUSTER

During the past year, a Master's thesis was completed on this subject by Peter M. Waltz. A circuit model was given using the arc current waveform. From these

we deduced the circuit parameters, calculated energy losses and thrust, and predicted efficiency. The model gives good quantitative agreement with parameters measured on a thrust stand.

This project is now concluded.

K. I. Thomassen

XX. APPLIED PLASMA RESEARCH*

B. Plasma Effects in Solids

Academic and Research Staff

Prof. A. Bers
Prof. G. Bekefi
Dr. E. V. George

Graduate Students

R. N. Wallace

RESEARCH OBJECTIVES

During the past year our studies have focused on the microwave emission from InSb at 77°K in applied electric (1-50 V/cm) and magnetic (1-10 kG) fields. We have shown that proper preparation of the ohmic contacts through which the electric field is applied can completely eliminate the spiked emission. Furthermore, spiked emission occurs only when the bad contact is also the negative potential end of the sample. Hence, hole-injection into the sample cannot play an important role, and we conclude that the emission is associated with breakdown resulting from localized high electric fields near the bad contact. Recently, we have found that even in the absence of contacts (when the electric field is induced into the sample) the noise emission (which is usually not spiked) occurs from localized regions in the material. This strongly suggests that material inhomogeneities, where localized high electric fields can develop, are responsible for the observed noise emission.

We plan to pursue these studies and establish the cause (and cure) of the noise emission from the bulk. A theoretical model of breakdown is being studied for explaining the observed threshold fields at the onset of noise emission.

Our theoretical studies of acoustic wave amplification have also continued. Our particular emphasis has been on the nonlocal interactions, which are important at microwave and higher frequencies, and the detailed effect on these interactions of the applied electric field. This work will be completed during the coming year.

A. Bers

1. EFFECT OF CONTACTS ON THE EMISSION FROM InSb

We have previously established the relation between noise emission and the quality of electrical contacts applied to n-type InSb.[1] Here we report further studies along these lines and describe the process of producing good contacts.

It has been observed that for samples with a poor contact on one end and a good contact on the other the emission thresholds were low when the poor contact acted as a cathode. When the poor contact acted as an anode, the emission thresholds were high and not many strong spikes were detected. This result is in agreement with the work of Kino and Thompson,[2] who found, by probing techniques, that the emission intensity was

*This work was supported by the National Science Foundation (Grant GK-10472).

very large near the cathode but very small (and nonexistent at threshold) near the anode. This is an important result, in that it implies that injection of holes from the poor contact into the bulk semiconductor was not responsible for the emission.

The sensitivity of the threshold characteristic with contact quality was further investigated by constructing a sample with diffused n^+-n contacts. A $1.1 \times 1.2 \times 9.9$ mm^3 sample of InSb was constructed with good contacts by using In(Te) solder. The threshold characteristics at 77°K were measured with the radiometer bridge[3] at four different frequencies, 0.5 GHz, 1.0 GHz, 1.5 GHz, and 2.0 GHz. The sample was then carefully removed from the sample holder and placed on a glass slide in a vacuum oven (ultimate pressure approximately 5 μ). The sample, including its electrical leads, was heated for 7 days at a temperature of approximately 150°C.

Using appropriate values of tellurium[4] at a temperature of 150°C, we find that the diffusion length L is approximately 10^{-4} cm. This is approximately the width of a Schottky barrier assumed to be formed at the metal-semiconductor interface.[5]

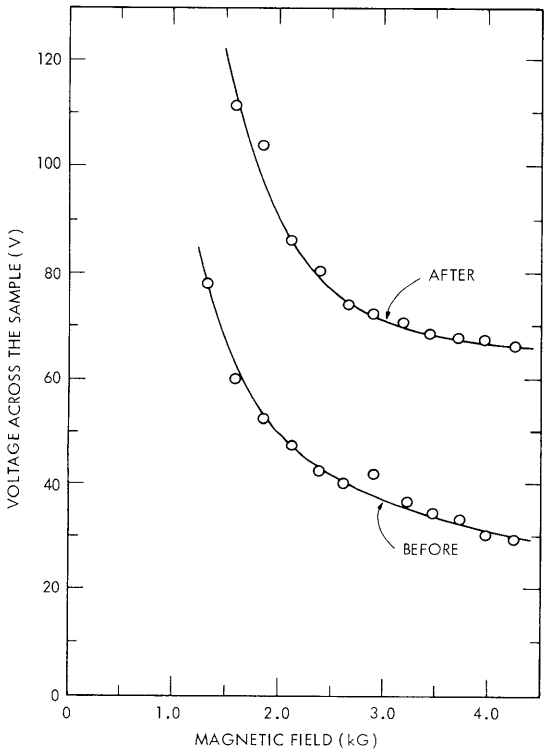

Fig. XX-6.

Threshold characteristics for an identical InSb semiconductor sample (S3-101), $1.1 \times 1.2 \times 9.9$ mm^3, with good contacts at 77°K, before and after diffusion of donor material (Te) into the bulk semiconductor at the contacts. The frequency of observation was 500 MHz. Threshold is defined as the amount of power equivalent to black-body radiation of ~3000°K.

After the diffusion process was completed, the sample was carefully remounted in the sample holder and the threshold characteristics were measured at the same four frequencies. Figure XX-6 illustrates the measured threshold characteristics for this sample, before and after the diffusion process at a frequency of 0.5 GHz. Very similar results were obtained at the other frequencies.

E. V. George

References

1. E. V. George and G. Bekefi, Appl. Phys. Letters 15, 33 (1969).
2. G. Kino and A. Thompson (private communication).
3. G. Bekefi, A. Bers, and S. R. Brueck, IEEE Trans., Vol. ED-14, No. 9, pp. 593-596 (September 1967).
4. O. Madelung and D. Meyerhofer, Physics of III-V Compounds (John Wiley and Sons, Inc., New York, 1964), p. 244.
5. E. V. George, Ph. D. Thesis, Department of Physics, M.I.T., September 1969.

2. FURTHER STUDIES OF MICROWAVE EMISSION FROM INDIUM ANTIMONIDE LOOPS

Further observations have been made of the microwave emission produced by round loops of n-type indium antimonide subjected to DC magnetic and induced RF electric fields. The basic experiment has been described in previous reports.[1-3]

Indium Antimonide Samples

Fourteen samples of n-type indium antimonide, cut from three different single crystals designated I, II, and III, were used in the work reported here. All samples were round loops with the same dimensions as in a preceding report,[4] where preliminary tests of samples 1 through 4 were described. The abrasive cutting machine[3] used to fabricate these samples has been modified by the author, and improved techniques for its operation have been developed. It is now possible to produce round-loop samples with dimensional tolerances of ±.001 in. or better before etching, and with surfaces that upon optical inspection appear free from all flaws except minor polishing scratches.

Table XX-1 summarizes a few relevant parameters for each of the samples. The specified electron density and mobility are the values at 77°K. Etching process "A" consisted in immersion of the sample for a period of 2-3 min in a solution of 1%-5% bromine in methanol. In etching process "B", samples were immersed for 10-15 min in a permanganate solution (1 HF, 1 CH_3COOH, 1 $KMnO_4$ 0.05M) developed by Witt.[5] Process "A" produced surfaces with a polished background and relatively large etch pits on the $(\bar{1}\bar{1}\bar{1})$ faces. Process "B" left very small etch pits on the sample surfaces. With the exception of sample 1 which was of unspecified crystallographic orientation, all samples were cut so that the plane of the loop coincided with the (111) plane. The samples were assigned numbers based on the order in which they were fabricated.

Table XX-1. Summary of sample parameters.

Sample	Crystal	Electron Density cm^{-3}	Mobility $cm^2/V\text{-}sec$	Etch Pit Density cm^{-2}	Etching Process	Surface Condition
1	I	$1.5\text{-}1.6\times10^{14}$	6×10^5	Unknown	A	Fair
2	II	$1.4\text{-}2.0\times10^{14}$	6×10^5	1900-2200	A	Bad
3					A	Fair
4					A	Fair
5					B	Bad
6					B	Bad
7					B	Good
8					B	Good
9					A	Good
10					B	Good
11	III	1.3×10^{14}	7×10^5	200	A	Good
12					B	Good
13					A	Good
14					B	Good

Experimental System

Some additions have been made to the equipment previously used for this series of experiments, but the basic system was essentially the same as that described in the most recent report.[3] Two different S-band superheterodyne receivers were used in addition to the original X-band receiver to allow observations of emission in the 2.6-3.2 GHz and 8.5-10.0 GHz frequency ranges. For the low signal levels normally encountered, these receivers tended to operate as square-law rather than linear detectors, and emission levels were plotted accordingly. By noting the level of the observed emission with respect to the receiver noise levels, and making use of the known noise figures of the receivers (typically 5-6 dB), rough estimates of the absolute emission intensity could be made. The receivers were equipped with synchronous detectors. Also, the video outputs of the receivers were monitored with oscilloscopes.

The mounting of the sample in the eccentric transmission line system previously

described[3] was modified so that the sample could be rotated about an axis perpendicular to the plane of the sample. Figure XX-7 shows the angles ϕ_R and ϕ_L in terms of which

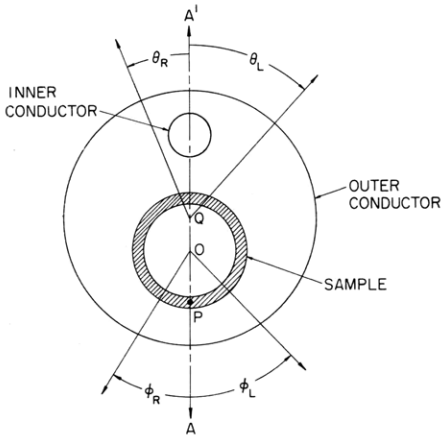

Fig. XX-7.
Definitions of the angles for describing the positions of the sample and the transmission line.

this rotation is defined. Rotation of the sample and the transmission line as a single unit about an axis normal to the plane of the page and passing through the point Q in Fig. XX-7 was also possible. The angles θ_R and θ_L measured this rotation.

Experimental Work

The modified eccentric transmission line system was used for all work reported here. Liquid nitrogen was employed to maintain the temperature of the round-loop samples at 77°K. Static magnetic fields were applied either parallel to or perpendicular to the plane of the sample. A pulsed 20-MHz RF magnetic field applied perpendicular to the plane of the sample induced the necessary electric field in the sample. A pulse width of 25 μs and a repetition rate of 100 pps were adopted as standard conditions for the present experiments. Rise and fall times for the induced electric field pulse were approximately 2-3 μs. "Electric field" values used in plotting data were the peak values attained during the applied pulse.

Microwave emission from the samples propagated along the eccentric transmission line and, after a transition, through standard waveguide sections to the X-band or S-band receivers. Measurements of wavelength at both X-band and S-band frequencies indicated that the emission propagated through the eccentric transmission line in a TEM mode.

a. Results with the Magnetic Field Parallel to the Sample Plane

Distribution of the Induced Electric Field. When the static magnetic field is applied parallel to the plane of a round-loop sample, the angle between this magnetic field and the RF induced current varies continuously with position along the sample. Because the longitudinal and transverse magnetoresistance effects in indium antimonide

are quite different in magnitude, the effective resistivity and the induced electric field must vary with position in the sample. If, however, the resistivity of the sample material is known as a function of the magnitude of the magnetic field and its direction with respect to the current flow, it is possible to determine the spatial distribution of the induced electric field.

Data for determining the induced electric field distribution were obtained from four-terminal DC magnetoresistance measurements made on two different rod-shaped samples of n-type indium antimonide. The rod-shaped samples, made from a crystal having electron concentration and mobility similar to those of the loop samples, were 1 mm square in cross section and approximately 20 mm long, with potential leads placed approximately 10 mm apart. The resistivity of each sample was recorded at 77°K as a function of the magnitude and direction of the applied magnetic field.

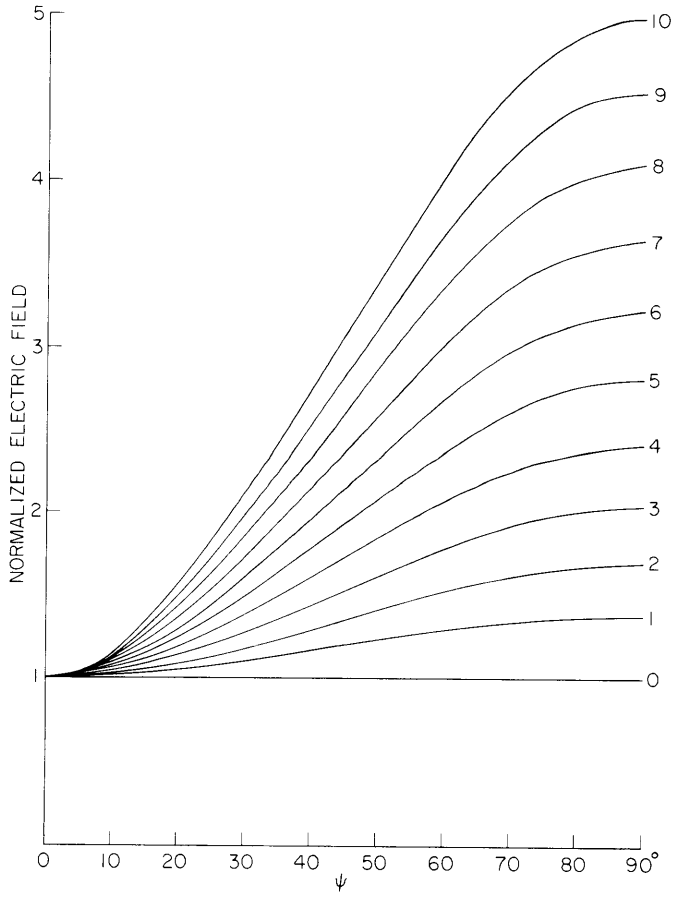

Fig. XX-8. Normalized electric field as a function of position on the sample, with static magnetic field applied parallel to the sample plane. The parameter identifying the different curves is the magnetic field in kG.

Figure XX-8 shows normalized induced electric field as a function of the position in a round-loop sample as determined from the magnetoresistance data. These data agreed fairly well with data of Frederikse and Hosler[6] for a material of similar electron density and mobility, and differences between the two samples tested here were typically less than 4%. The induced electric field is normalized to unity at the position of minimum electric field, where the static magnetic field and the local current flow are parallel. The acute angle formed between the directions of the static magnetic field and the local current flow is denoted ψ. The parameter that distinguishes the separate curves in Fig. XX-8 is the applied magnetic field in kG.

Microwave Emission from Round-Loop Samples. Samples 1 through 7 were tested for emission with the static magnetic field applied parallel to the sample plane. Of these, sample 3 produced no observable emission at X-band (8.5-10.0 GHz) or S-band (2.6-3.2 GHz) frequencies. Samples 1 and 7 produced emission levels so close to the receiver noise levels that quantitative data could not be taken. Samples 2, 4, 5 and 6 produced emission of sufficient strength to yield useful data. The maximum electric and magnetic fields normally employed in searching for emission were 58 V/cm (spatial median) and 10 kG.

[It was found convenient to define the "spatial median" of the induced electric field as the average of the maximum and minimum field values in the sample. This choice produced a fairly good correlation between results of experiments in which the magnetic field was applied parallel to the plane of the sample and those in which it was applied perpendicular to the plane of the sample. Good agreement was also obtained with previous studies of square-loop samples. If the spatial median electric field and the magnetic field are known, the actual electric field distribution in the sample can be determined with the use of Fig. XX-8. Unless stated otherwise, "electric field" values given in the rest of this section are to be interpreted as spatial median values.]

The samples that produced emission showed electric and magnetic field threshold characteristics similar to those reported previously.[2, 3] With an applied magnetic field of 10 kG, the electric field at threshold ranged from approximately 11 to 49 V/cm in the different samples tested. Threshold electric fields increased to 50-60 V/cm when the magnetic field was lowered to 3-4 kG. The microwave emission usually appeared as a flat-topped pulse coincident with the applied electric field pulse. In general, we found that emission levels increased as the electric and magnetic fields were raised above their threshold values. There seemed to be a tendency for the emission level to saturate for magnetic fields in excess of 8 kG. Data demonstrating this behavior for a typical sample are shown in Fig. XX-9. The maximum emission level produced by this sample at 9.3 GHz corresponded to that from a black body having a temperature of $\sim 10^5$ °K.

As samples were rotated in the eccentric transmission line, the microwave emission

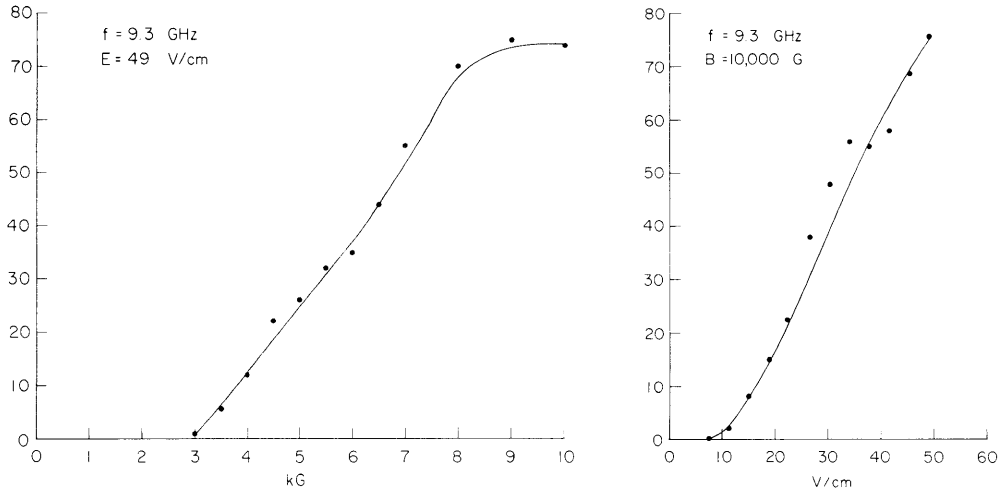

Fig. XX-9. Emission from sample 6 at 9.3 GHz as a function of electric and magnetic fields, with $\phi_R = 65°$ and $\theta_L = 30°$. The ordinate in these graphs and in those that follow represents microwave power in arbitrary units.

level observed at either X-band or S-band frequencies varied. Depending on the sample, this variation of the emission could be relatively complicated in structure, displaying several peaks as the sample moved from $\phi_L = 180°$ through $\phi = 0$ to $\phi_R = 180°$. Such complicated structures are shown in Figs. XX-10 and XX-11. Alternatively, only a single peak might appear as a particular sample was rotated through 360°. Such behavior is indicated by Figs. XX-12 and XX-13. In general, the different variations in emission level at X-band and S-band frequencies produced by rotating a particular sample were strongly correlated but not identical. A comparison of Figs. XX-12 and XX-13 shows this. This result may reflect differences in microwave coupling in the two frequency bands.

As the position of the transmission line was changed from $\theta_L = 90°$ through $\theta = 0$ to $\theta_R = 90°$, thereby changing the orientation of the static magnetic field with respect to both the sample and the microwave system, the pattern of emission as a function of ϕ tended to translate along the ϕ axis. For example, a peak of emission that appeared for a particular combination of θ and ϕ might shift by 30° in ϕ as θ was changed by 30°. This shift in ϕ would be just sufficient to restore the original orientation of the sample with respect to the static magnetic field. This behavior is demonstrated most clearly in Fig. XX-12, and is present to a lesser extent in Figs. XX-10, XX-11, and XX-13. Part of the problem in obtaining clear results may be that the microwave coupling between the transmission line and the assumed localized microwave sources in the sample shifts as θ and ϕ are altered to maintain a constant orientation between the sample and the magnetic field.

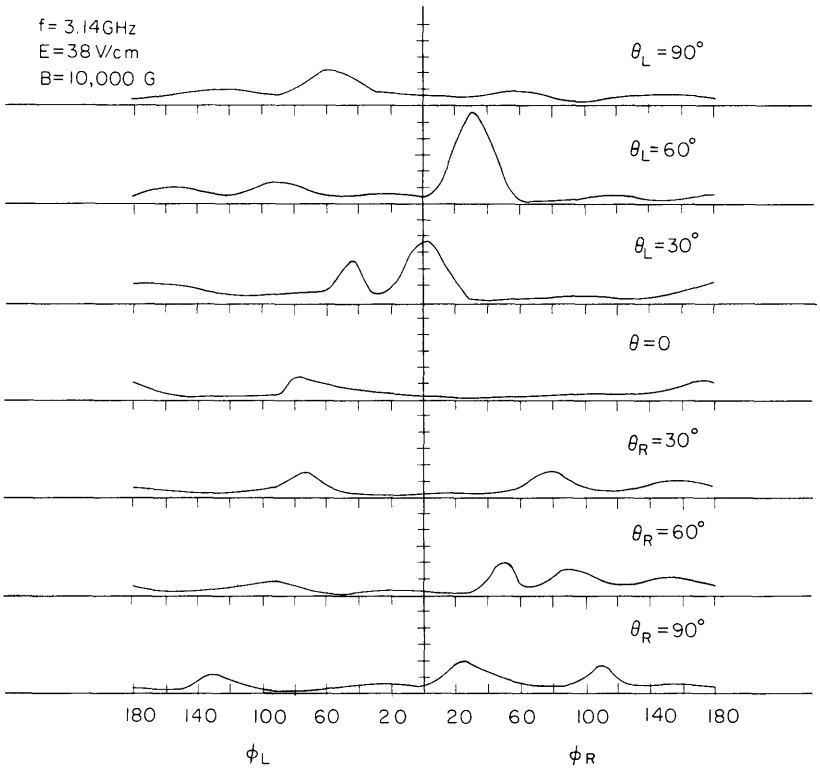

Fig. XX-10. Emission from sample 2 at 3.14 GHz as a function of θ and ϕ with fixed electric and magnetic fields.

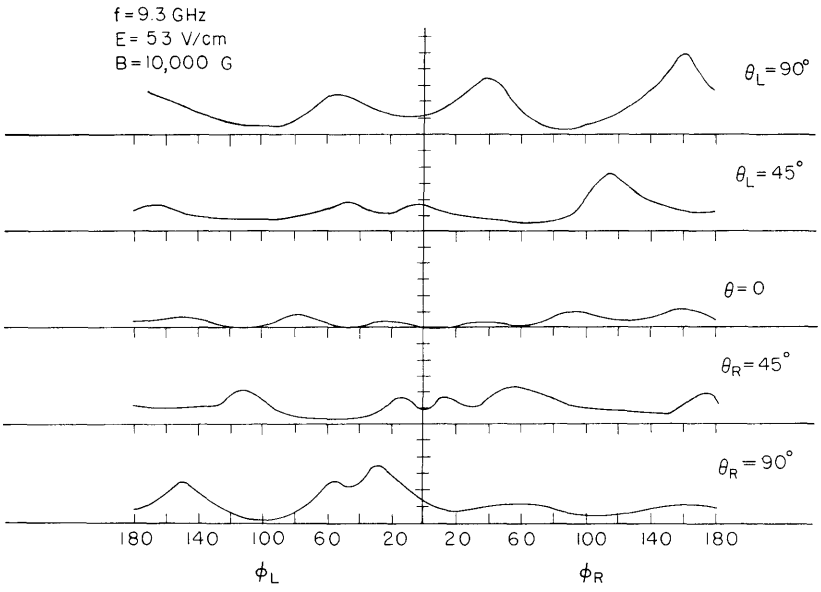

Fig. XX-11. Emission from sample 5 at 9.3 GHz as a function of θ and ϕ with fixed electric and magnetic fields.

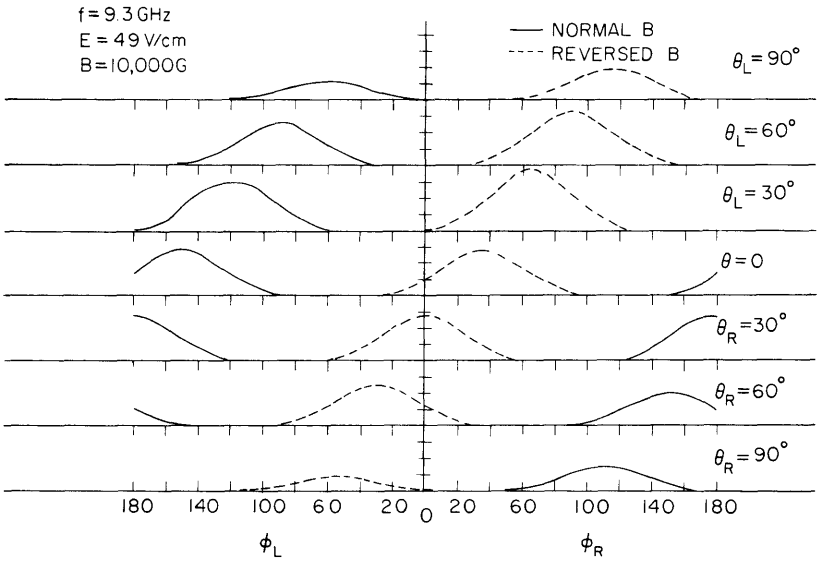

Fig. XX-12. Emission from sample 6 at 9.3 GHz as a function of θ and ϕ with fixed electric and magnetic fields. The solid and dashed curves in this and following figures represent emission levels for opposite magnetic field polarities.

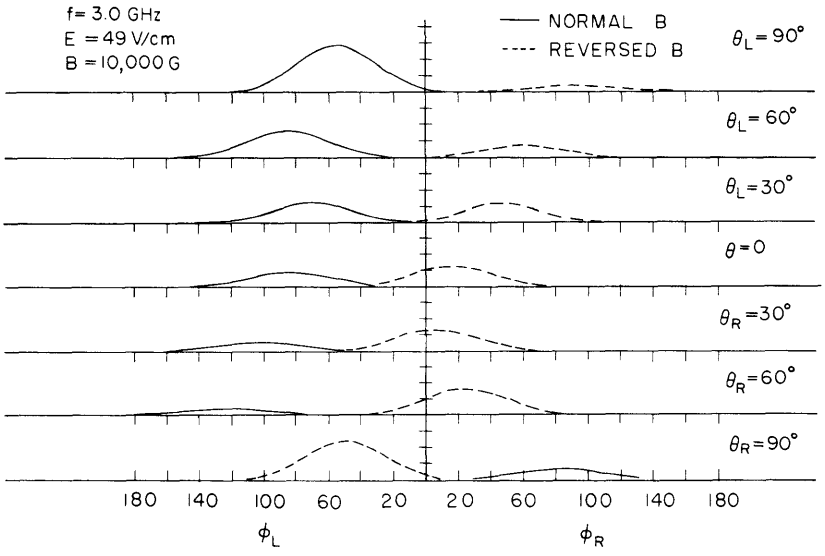

Fig. XX-13. Emission from sample 6 at 3.0 GHz as a function of θ and ϕ with fixed electric and magnetic fields.

Pronounced changes in emission level occurred for most of the round-loop samples upon reversal of the static magnetic field. For sample 6, the emission level at 9.3 GHz changed by approximately 20 dB when the magnetic field was reversed. Following reversal of the magnetic field, the single peak of emission could be recovered by rotating the sample through approximately 180°, as is shown in Figs. XX-12 and XX-13. For samples with a complicated dependence of emission level on ϕ, the change following reversal of the magnetic field was typically from 3 dB to 10 dB.

From all of these results, one strong point emerges. If the samples had been homogeneous and isotropic, the emission level would not have varied with sample rotation. But the observed emission level did vary with sample rotation. The form of this variation differed from sample to sample and was unrelated to the known crystal anisotropy. We must therefore conclude that the emission occurs from localized regions associated with inhomogeneities in the sample material.

Furthermore, because both polarities of the electric field are available during the 20-MHz RF pulses used in these experiments, nonreciprocal effects related only to the magnetic field direction must be found to explain the change of emission level caused by magnetic field reversal.

b. Results with the Magnetic Field Perpendicular to the Sample Plane

A somewhat simpler experimental situation prevails when the static magnetic field is applied perpendicular to rather than parallel to the plane of the sample. In this case, the magnetic field is everywhere perpendicular to the direction of the RF induced current, and the induced electric field is macroscopically uniform.

Samples 1, 3, and 5 through 14 were tested with the static magnetic field perpendicular to the sample plane. Of these, samples 1, 5, 6, 8, 10, 11, and 13 produced observable emission. The electric and magnetic fields used in searching for emission were typically 54-56 V/cm and 5 kG. When microwave emission was found, it displayed electric and magnetic field threshold characteristics similar to those found both in previous work[2,3] and in the present experiments with the magnetic field applied parallel to the sample plane. Threshold electric fields for the samples that emitted ranged from ~18-48 V/cm (typically 30-35 V/cm) with a magnetic field near 5 kG. Using the maximum electric field, 54-56 V/cm, we found magnetic field thresholds from ~2800-4000 G. For a given sample, the threshold fields for S-band emission were very slightly smaller than those for X-band emission. The observed emission intensity increased monotonically as either the electric or the magnetic field was raised above threshold conditions. Figure XX-14 shows this dependence of the observed X-band and S-band emission upon electric and magnetic field strength for a typical sample. The results shown are generally similar to those of Fig. XX-9, but the maximum magnetic field available in the

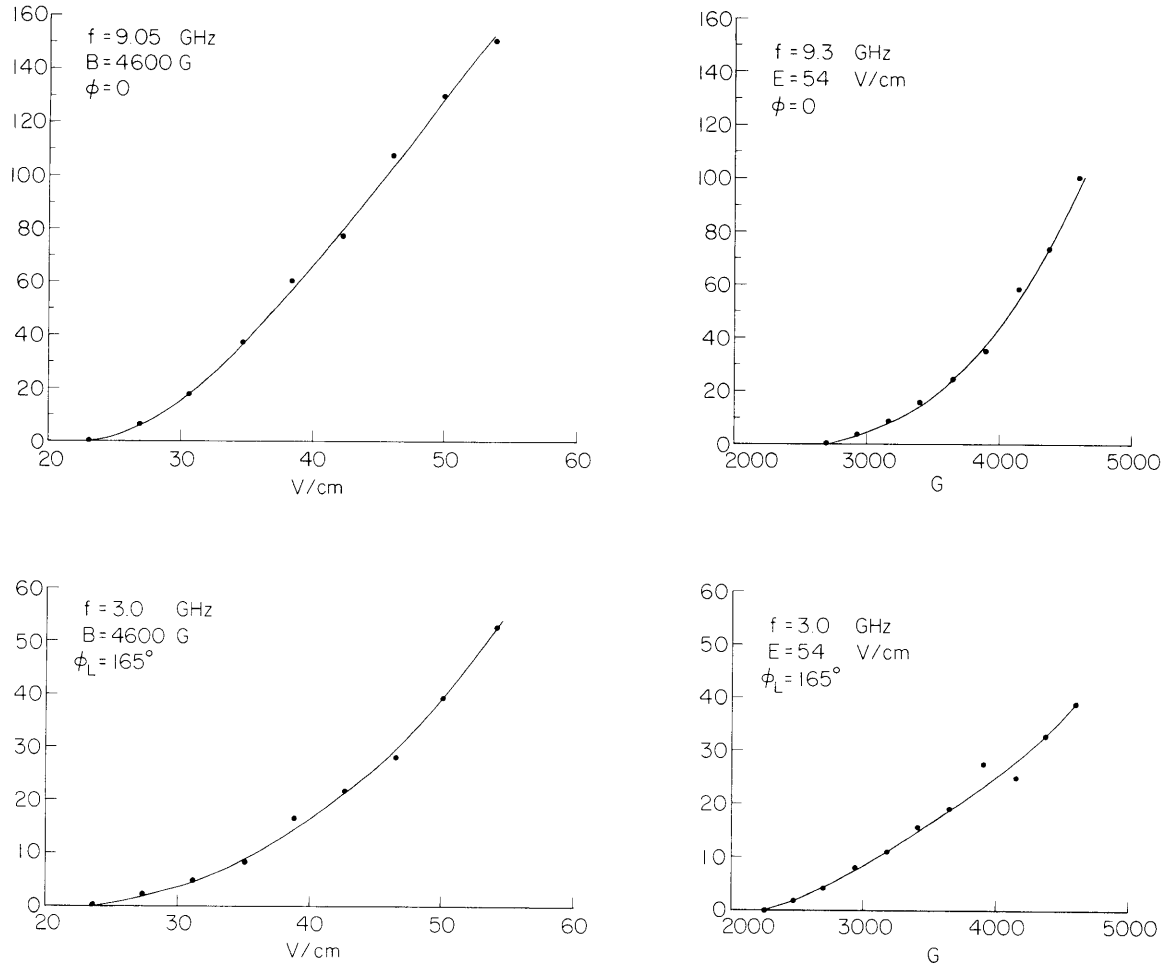

Fig. XX-14. Emission from sample 11 at 9.05 GHz and 3.0 GHz as a function of electric and magnetic fields with $\theta = 0$.

present case did not cause saturation of the emission level. The maximum emission level that could be produced at either X-band or S-band frequencies was approximately equal to that from a black body with a temperature of 2×10^4 °K. The reduction of the maximum magnetic field from 10 kG to 5 kG for this set of experiments may well have accounted for this lower emission level.

Variations of the observed emission levels with rotations of the sample and the transmission line were somewhat more simple with the static magnetic field applied perpendicular to rather than parallel to the sample plane. As was expected, rotation of the transmission line (variation of θ in Fig. XX-7) produced negligible changes in the emission. Such changes as were present could have been the result of imperfect magnetic field alignment. There were in general substantial variations in the observed emission level as the sample was rotated. This again supported the conclusion that the emission originates in localized regions in the sample.

Most samples exhibited two broad peaks of emission approximately 180° apart as rotation from $\phi_L = 180°$ through $\phi = 0$ to $\phi_R = 180°$ was completed. The ratio of maximum-to-minimum emission level during rotation was typically 3-10 dB. As was the case in the experiments with the magnetic field parallel to the sample plane, the variations of X-band and S-band emission with ϕ were strongly correlated, but not identical. Data for a sample showing a relatively pronounced pattern of emission peaks are shown in Fig. XX-15. Occasionally, a sample produced relatively constant emission levels and showed a poorly defined pattern of emission peaks as ϕ varied. Data for such a sample are shown in Fig. XX-16. There is some preliminary evidence that samples showing relatively small variations in emission level when rotated in the present experiments produce complicated patterns of emission as a function of ϕ when tested with the magnetic field parallel to the sample plane. Also, a pronounced variation of emission with ϕ in the present experiments would signal a relatively simple pattern of emission as a function of ϕ in the earlier case. Distinctions between these two types of behavior, if supported by future experiments, might form a means for deciding respectively whether multiple or single localized microwave sources existed in a particular sample.

As is indicated by Figs. XX-15 and XX-16, the emission levels did not change greatly with reversal of the static magnetic field. This contrasts with the results shown in Figs. XX-12 and XX-13 when the magnetic field was applied parallel to the sample plane.

Discussion

It is now fairly clear that the microwave emission from indium antimonide loops observed here is produced by localized sources associated with random inhomogeneities in the sample material. This conclusion is supported by the behavior of the observed emission, and reinforced by the fact that both emitting and nonemitting samples are produced by identical fabrication techniques.

Optical inspection of the sample surfaces does have some statistical value in predicting whether a given sample will produce observable emission in the present experimental system. Previous expectations[3] for the reliability of this test were not realized, however. Of 6 samples judged to have "fair" or "bad" surfaces, 5 produced emission. Among the 8 samples having "good" surfaces, 4 produced observable emission. It thus appears that elimination of surface damage will not necessarily exclude the microwave emission.

For those round-loop samples producing emission, the threshold electric and magnetic fields were of the same order as or smaller than the threshold fields previously reported[2, 3] for intact square-loop samples. From the present work, it thus appears that the regions of higher electric field in the corners of the square-loop samples were

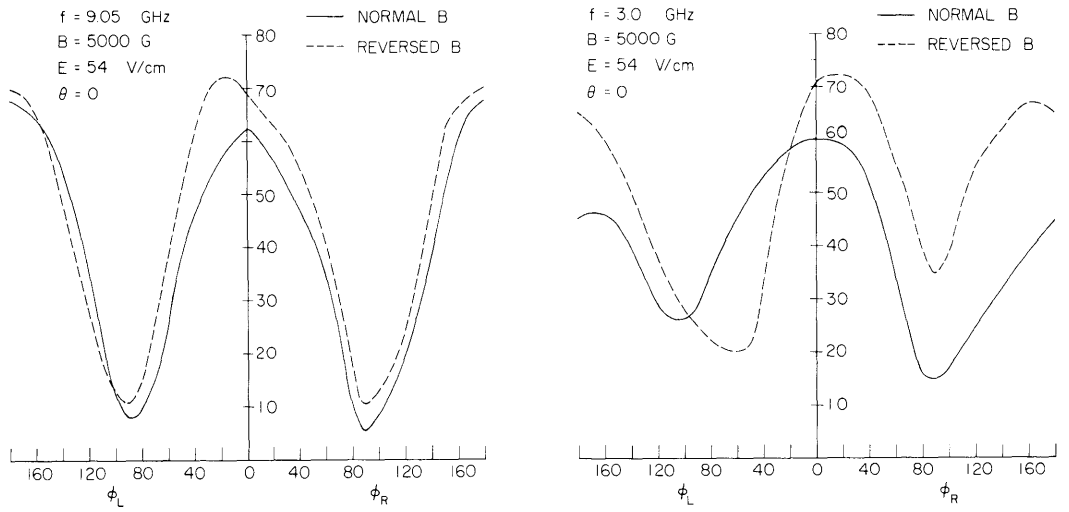

Fig. XX-15. Emission from sample 8 at 9.05 GHz and 3.0 GHz as a function of ϕ with fixed electric and magnetic fields, and with $\theta = 0$.

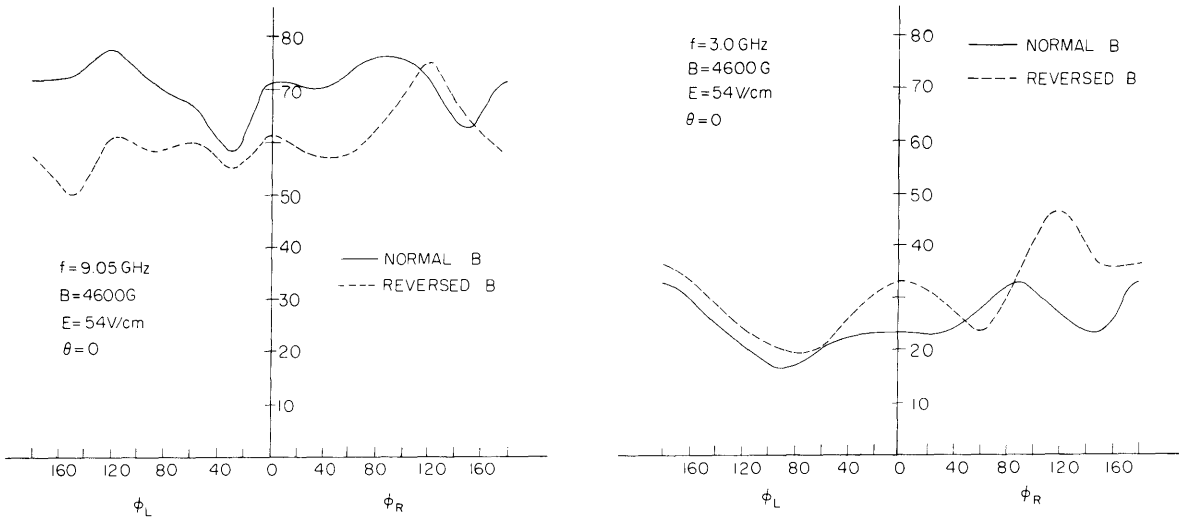

Fig. XX-16. Emission from sample 13 at 9.05 GHz and 3.0 GHz as a function of ϕ with fixed electric and magnetic fields, and with $\theta = 0$.

not a major emission-producing factor.

The threshold fields in the present work were of the same order as or larger than those reported by George[7] for rod-shaped samples with "good" contacts, and much larger than those reported for rod-shaped samples with "bad" contacts. The flaws occurring randomly in the bulk thus seem somewhat less effective in producing microwave emission than the gross inhomogeneity created by a contact.

Work is now under way to develop a model for the microwave emission process in indium antimonide based on the presence of inhomogeneities in the bulk.

R. N. Wallace

References

1. R. N. Wallace, "Low-Field Microwave Emission from Contactless Indium Antimonide Samples," Quarterly Progress Report No. 87, Research Laboratory of Electronics, M.I.T., October 15, 1967, pp. 121-129.
2. R. N. Wallace, "Effects of Contacts on Low-Field Microwave Emission from Indium Antimonide Loops with Induced Electric Fields," Quarterly Progress Report No. 89, Research Laboratory of Electronics, M.I.T., April 15, 1968, pp. 151-155.
3. R. N. Wallace, "Microwave Emission from Indium Antimonide Loops," Quarterly Progress Report No. 94, Research Laboratory of Electronics, M.I.T., July 15, 1969, pp. 190-195.
4. R. N. Wallace, Quarterly Progress Report No. 94, op. cit., see Fig. XI-4, p. 190.
5. A. F. Witt, J. Electrochem. Soc. 114, 298 (1967).
6. H. P. R. Frederikse and W. R. Hosler, Phys. Rev. 108, 1136 (1957).
7. E. V. George, "Microwave Instabilities in a Semiconductor Subjected to DC Electric and Magnetic Fields," Quarterly Progress Report No. 91, Research Laboratory of Electronics, M.I.T., October 15, 1968, pp. 154-158.

XX. APPLIED PLASMA RESEARCH*

C. Plasma Physics and Engineering

Academic and Research Staff

Prof. R. A. Blanken	Prof. E. P. Gyftopoulos	Prof. W. M. Manheimer
Prof. T. H. Dupree	Prof. L. M. Lidsky	Dr. E. Oktay

Graduate Students

D. P. Hutchinson	C. A. Primmerman	J. E. Robinson
M. A. Lecomte		C. E. Wagner

RESEARCH OBJECTIVES

1. Nonlinear Plasma Theory

We are attempting to compute the wave-number spectrum of the distribution function of particles that are resonant with waves. Particles moving together at the same velocity develop into long-lived clumps that introduce an enhanced "discreteness" into the plasma. The enhanced discreteness in turn produces an increase in all collision-related effects such as resistivity, radiation, and diffusion. We intend to investigate these effects for a number of specific cases.

T. H. Dupree

2. Studies of Velocity Space Instabilities in Hot-Electron Plasmas

Theoretical analyses of various velocity space instabilities that can occur in relativistic electron plasmas continue. In particular, the two-component instability is under investigation.

R. A. Blanken

3. Plasma Studies in a Small-Scale Levitron

A small Levitron type of plasma confinement has been constructed and is in operation. Plasma is produced via electron-cyclotron resonance heating. Studies of the plasma confinement in Levitron geometry are proceeding.

L. M. Lidsky

4. Stuffed Cusp Experiment

Our original objective in this work was the investigation of the stability boundaries of hot-electron plasmas in several magnetic field structures. The plasma, formed by the beam-plasma interaction, has turned out to be very complex. We have therefore turned to a simpler version of the original problem – an attempt to measure and

*This work is supported by the National Science Foundation (Grant GK-10472).

understand the nature and stability boundaries of the observed electron-cyclotron frequency instabilities. We have developed new ultrahigh-frequency probes and are using these to investigate the properties of single-wave packets.

C. E. Wagner, L. M. Lidsky

5. Velocity Distribution in Mirror Plasmas

We have developed a new experimental technique for measuring the electron velocity distribution near the loss-cone edge in hot-electron mirror plasmas. The results will be used to compute the $T_\perp / T_i$ ratio in beam-generated plasmas.

C. A. Primmerman, L. M. Lidsky

6. Pulsed 10.6 μ Laser Systems

We are investigating several schemes for increasing the Q-switch power output of the 10.6 μ H_2-CO_2-He laser systems. The most promising idea at the moment involves using the afterglow of a high-pressure strongly excited discharge. The objective of this study, in addition to our increased understanding of the dynamics of the N_2-CO_2-He excitation transfer processes, is the development of simple techniques capable of producing pulses in the 0.1-1.0 MW peak-power range.

D. P. Hutchinson, L. M. Lidsky

7. The nonlinear stabilization of a variety of linearly unstable waves that propagate at multiples of the electron or ion cyclotron frequencies is being studied theoretically. Many of these waves become damped if real ω is shifted by a small amount $\Delta\omega \ll \omega$. Such waves are easily stabilized if nonlinear effects broaden the wave-particle resonance by an amount $\Delta\omega$.

T. H. Dupree

8. Plasma Transport in Turbulent Columns

Although it is generally agreed that fluctuating electric fields are the cause of experimentally observed enhanced plasma transport, the expected quantitative relations between the magnitude and frequency of the fluctuations and the speed and direction of transport are not often satisfied. We have developed a new technique for the direct measurement of diffusion flux and are using it to investigate plasma flows in the plasma column. We are investigating the possibilities of using "Lisitano coils" to generate a weakly turbulent plasma for these studies. Preliminary measurements indicate that the plasma density and temperature generated in our 3-m plasma device (HCD-III) by Lisitano coils are well suited to probe diagnostics and just turbulent enough to be interesting.

J. E. Robinson, E. Oktay, L. M. Lidsky